

## Modul 1

### Introduction to nanophotonics (photonic crystals) Transfer-matrix method

#### Structural colour

Nature has always been an invaluable source of inspiration for technological progress. Great scientific revolutions were started by the work of men such as Leonardo da Vinci and Galileo Galilei, who were able to learn from nature and apply their knowledge most effectively. The process of transferring the ingenious solutions evolved by some species into engineered devices is now an established and autonomous discipline known as biomimetics. Due to advances in the fabrication technologies of nanometer-scale optical devices, biomimetics has expanded into the field of non-classical optics. This gives an opportunity for engineers and zoologists to learn from nature in a mutually beneficial partnership. Engineers can draw inspiration from the ways in which Nature produces fascinating optical effects and zoologists can apply the quantitative theoretical methods developed in optical engineering to understand the phenomenology of their specimens. The development of expertise brought about by this interaction has already resulted in commercially available products. The surface of some optical discs for data storage and certain surface-relief volume phase holograms share the designs and functionality of the microstructures found in the eye of moths and on the wings of butterflies.

Visual appearance is one of the areas in which nature has evolved smart optical solutions. Through interference of light reflected or diffracted by minute features, many organisms are able to generate structural colour. Different optical effects are generated by arrangements of biomaterial on the surface of various organisms. The study of structural colour is old. Observations of optical interference effects have been reported by illustrious scientists, whose ingenuity has laid the foundations of modern science. In a time when the wonders of nanotechnologies were not conceivable, those researchers turned to nature and used their intuition to identify, via their phenomenology, optical microstructures which they could not possibly see.

Hooke [1] in 1665 when considering the optical properties of silverfish (*Ctenopoma* sp.) observed:  
. . . the appearance of so many several shells or shields that cover the whole body, every one of these shells are covered or tiled over with a multitude of transparent scales, which, from the multiplicity of their reflecting surfaces, make the whole animal a perfect pearl colour.



Newton dedicated his Second book of Opticks [2] to the optics of thin transparent bodies and in one of his propositions he observed:

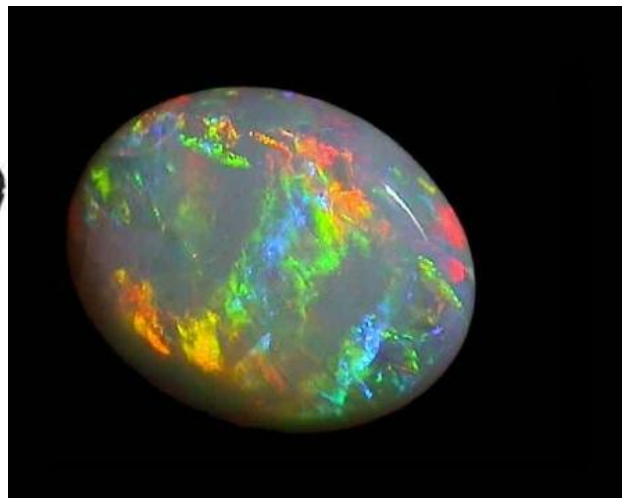
[...] The finely colour'd Feathers of some Birds, and particularly those of Peacocks Tails, do, in the very same part of the Feather, appear of several Colours in several Positions of the eye, after the very same manner that thin Plates were found to do [...] and therefore their Colours arise from the thinness of the transparent parts of the Feathers; that is, from the



slenderness of the very fine Hairs, or Capillamenta, which grow out of the sides of the grosser lateral Branches or Fibres of those Feathers.

Acknowledgment of the intrinsic relation between structural colour and the interaction of light with microscopic objects emerged in those early days, together with the scientists' new found interest in the phenomena of interference, refraction and reflection, and understanding of the nature of light.

A wide variety of diffractive structures is found in Nature. These are specialized devices functioning as reflectors in most cases, but also as transmitters. Depending on their function, they may have different periods, some of sizes smaller than the wavelength of the relevant radiation (zero-order structures), or be periodic along two directions on the corrugated surface. Colour can also be generated by a three-dimensional distribution of dielectric material such as is found in crystal lattices. Extremely regular lattices, in fact face-centered cubic crystals of inverted spheres, occur in iridescent butterflies.



Similarly, structural colour is produced by opals, iridescent stones made of



ordered grains of amorphous silica, which have an internal structure periodic in three dimensions. Often the term opalescence is used in this case instead of iridescence. Naturally, we expect the relevant interaction between light and three-dimensional structures to take place in the inside of the samples, but it must be emphasized that this also applies to surface diffractive structures. Even in specimens which we regard as surface, one- or two-dimensional structures, the electromagnetic field often penetrates deeply inside the periodic arrangement of dielectric material and the chromatic effect results from the extension of the waves deep within the structure. For this reason, they must be regarded as volume diffractive structures rather than surface ones. The cat tapetum or the hair of the sea mouse are examples of systems in which the iridescence is the result of interdependent diffraction and interference processes. The striking intensity and amazing effects of structural colour in Nature are achieved with materials, and control over the geometries, that by some human standards would be regarded as rather limited. The occurring contrasts in index of refraction are less than 1.83 and therefore only a small reflection can take place at individual boundaries between two materials for small angles of incidence.

### **Thin films**

Thin-film optics is the branch of optics that deals with very thin structured layers of different materials. In order to exhibit thin-film optics, the thickness of the layers of material must be on the order of the wavelengths of visible light (about 500 nm). Layers at this scale can have remarkable reflective properties due to light waveinterference and



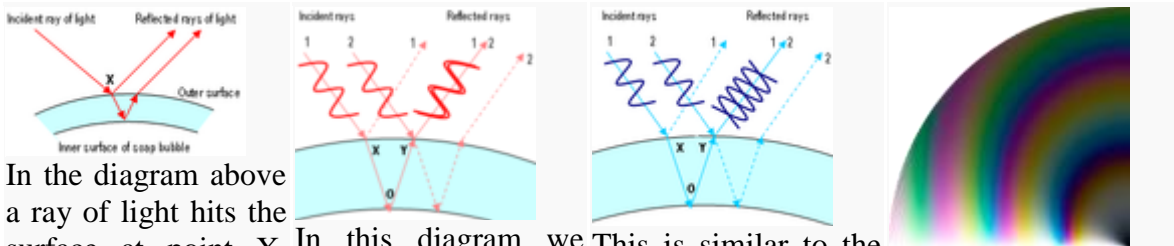
the difference in refractive index between the layers, the air, and the substrate. These effects alter the way the optic reflects and transmits light. This effect is observable in soap bubbles and oil slicks.

The iridescent colours of soap bubbles are caused by interfering light waves and are determined by the thickness of the film. They are not the same as rainbow colours but are the same as the colours in an oil slick on a wet road.

As light impinges on the film, some of it is reflected off the outer surface while some of it enters the film and reemerges after being reflected back and forth between the two surfaces. The total reflection observed is determined by the interference of all these reflections. Since each traversal of the film incurs a phase shift proportional to the thickness of the film and inversely proportional to the wavelength, the result of the interference depends on these two quantities. So at a given thickness, interference is constructive for some wavelengths and destructive for others, so that white light impinging on the film is reflected with a hue that changes with thickness.

A change in colour can be observed while the bubble is thinning due to evaporation. Thicker walls cancel out red (longer) wavelengths, causing a blue-green reflection. Later, thinner walls will cancel out yellow (leaving blue light), then green (leaving magenta), then blue (leaving a golden yellow). Finally, when the bubble's wall becomes much thinner than the wavelength of visible light, all the waves in the visible region cancel each other out and no reflection is visible at all. When this state is observed, the wall is thinner than about 25nm, and is probably about to pop. This phenomenon is very useful when making or manipulating bubbles as it gives an indication of the bubble's fragility.

Interference effects also depend upon the angle at which the light strikes the film, an effect called iridescence. So, even if the wall of the bubble were of uniform thickness, one would still see variations of colour due to curvature and/or movement. However, the thickness of the wall is continuously changing as gravity pulls the liquid downwards, so bands of colours that move downwards can usually also be observed.



In the diagram above a ray of light hits the surface at point X. Some of the light is reflected, but some travels through the bubble wall and is reflected at the other side.

When light directed from low index material strikes a high index material (air to film), there is a 180 degree phase

In this diagram we look at two rays of red light (rays 1 and 2). Both rays are split as before and follow two possible paths, but we are interested only in the paths that are represented by the solid lines. Consider the ray emerging at Y. It consists of two rays on top of one another:

This is similar to the previous diagram except the wavelength is different. This time  $XOY$  is not an integer multiple of the wavelength of blue light and so ray 1 and 2 arrive at y out of step. The troughs of ray 1 line up with the humps of ray 2 and the two rays cancel

This computed image shows the colours reflected by a thin film of water illuminated by unpolarized white light. The radius is proportional to the thickness of the film, and the polar angle is the angle of incidence.

shift just from the the bit that went each other out. The reflection (a "hard" through the bubble overall effect is that reflection). So the wall for ray 1 and the no blue light will be film thicknesses bit that was reflected reflected for this discussed for red and off the outer wall of thickness of bubble. blue light in the ray 2. Ray one has panels to the right are travelled XOY further incorrect by half a than ray 2. Since wavelength. XOY happens to correspond to an integer multiple of the wavelength of red light, the two rays are in phase (the humps and troughs are together).

### **Anti-reflective coatings**

Anti-reflective coatings are a type of optical coating applied to the surface of lenses and other optical devices to reduce reflection. This improves the efficiency of the system since less light is lost. In complex systems such as a telescope, the reduction in reflections also improves the contrast of the image by elimination of stray light. This is especially important in planetary astronomy. In other applications, the primary benefit is the elimination of the reflection itself, such as a coating on eyeglass lenses that makes the eyes of the wearer more visible, or a coating to reduce the glint from a covert viewer's binoculars or telescopic sight.

Many coatings consist of transparent thin film structures with alternating layers of contrasting refractive index. Layer thicknesses are chosen to produce destructive interference in the beams reflected from the interfaces, and constructive interference in the corresponding transmitted beams. This makes the structure's performance change with wavelength and incident angle, so that color effects often appear at oblique angles. A wavelength range must be specified when designing or ordering such coatings, but good performance can often be achieved for a relatively wide range of frequencies: usually a choice of IR, visible, or UV is offered.

The simplest form of antireflection coating was discovered by Lord Rayleigh in 1886. The optical glass available at the time tended to develop a tarnish on its surface with age, due to chemical reactions with the environment. Rayleigh tested some old, slightly tarnished pieces of glass, and found to his surprise that they transmitted more light than new, clean pieces. The tarnish replaces the air-glass interface with two interfaces: an air-tarnish interface and a tarnish-glass interface. Because the tarnish has an index of refraction between that of glass and that of air, each of these interfaces exhibits less reflection than the air-glass interface did, and in fact the total of the two reflections is less than that of the "naked" air-glass interface.

Interference-based coatings were invented in November 1935 by Alexander Smakula, who was working for the Carl Zeiss optics company. Anti-reflection coatings were a German military secret until the early stages of World War II.

There are two separate causes of optical effects due to coatings, often called thick film and thin film effects. Thick film effects arise because of the difference in the index of refraction between the layers above and below the coating (or film); in the simplest case, these three layers are the air, the coating, and the glass. Thick film coatings do not depend on how thick the coating is, so long as the coating is much thicker than a wavelength of light. Thin film effects arise when the thickness of the coating is approximately the same as a quarter or a half a wavelength of light. In this case, the reflections of a steady source of light can be made to add destructively, and hence reduce reflections by a separate mechanism. In addition to depending very much on the thickness of the film, and the wavelength of light, thin film coatings depend on the angle at which the light strikes the coated surface.

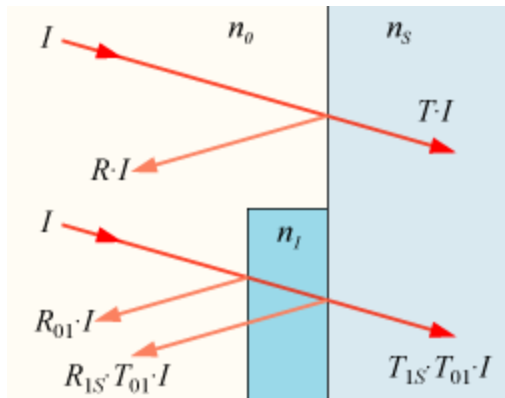
### Reflection

Whenever a ray of light moves from one medium to another (for example, when light enters a sheet of glass after travelling through air), some portion of the light is reflected from the surface (known as the interface) between the two media. This can be observed when looking through a window, for instance, where a (weak) reflection from the front and back surfaces of the window glass can be seen. The strength of the reflection depends on the refractive indices of the two media as well as the angle of the surface to the beam of light. The exact value can be calculated using the Fresnel equations.

When the light meets the interface at normal incidence (perpendicularly to the surface), the intensity of light reflected is given by the reflection coefficient or reflectance,  $R$ :

$$R = \left( \frac{n_0 - n_s}{n_0 + n_s} \right)^2,$$

where  $n_0$  and  $n_s$  are the refractive indices of the first and second media, respectively. The value of  $R$  varies from 0.0 (no reflection) to 1.0 (all light reflected) and is usually quoted as a percentage. Complementary to  $R$  is the transmission coefficient or transmittance,  $T$ . If absorption and scattering are neglected, then the value  $T$  is always  $1-R$ . Thus if a beam of light with intensity  $I$  is incident on the surface, a beam of intensity  $RI$  is reflected, and a beam with intensity  $TI$  is transmitted into the medium.



For the simplified scenario of visible light travelling from air ( $n_0 \approx 1.0$ ) into common glass ( $n_s \approx 1.5$ ), value of  $R$  is 0.04, or 4% on a single reflection. So at most 96% of the light ( $T=1-R=0.96$ ) actually enters the glass, and the rest is reflected from the surface. The amount of light reflected is known as the reflection loss.

In the more complicated scenario of multiple reflections, say with light travelling through a window, light is reflected both when going from air to glass and at the other side of

the window when going from glass back to air. The size of the loss is the same in both cases. Light also may bounce from one surface to another multiple times, being partially reflected and partially transmitted each time it does so. In all, the combined reflection coefficient is given by  $2R/(1+R)$ . For glass in air, this is about 7.7%.)

### Rayleigh's film

As observed by Lord Rayleigh, a thin film (such as tarnish) on the surface of glass can reduce the reflectivity. This effect can be explained by envisioning a thin layer of material with refractive index  $n_1$  between the air (index  $n_0$ ) and the glass (index  $n_s$ ). The light ray now reflects twice: once from the surface between air and the thin layer, and once from the layer-to-glass interface.

From the equation above, and the known refractive indices, reflectivities for both interfaces can be calculated, and denoted  $R_{01}$  and  $R_{1s}$ , respectively. The transmission at each interface is therefore  $T_{01} = 1 - R_{01}$  and  $T_{1s} = 1 - R_{1s}$ . The total transmittance into the glass is thus  $T_{1s}T_{01}$ . Calculating this value for various values of  $n_1$ , it can be found that at one particular value of optimum refractive index of the layer, the transmittance of both interfaces is equal, and this corresponds to the maximum total transmittance into the glass.

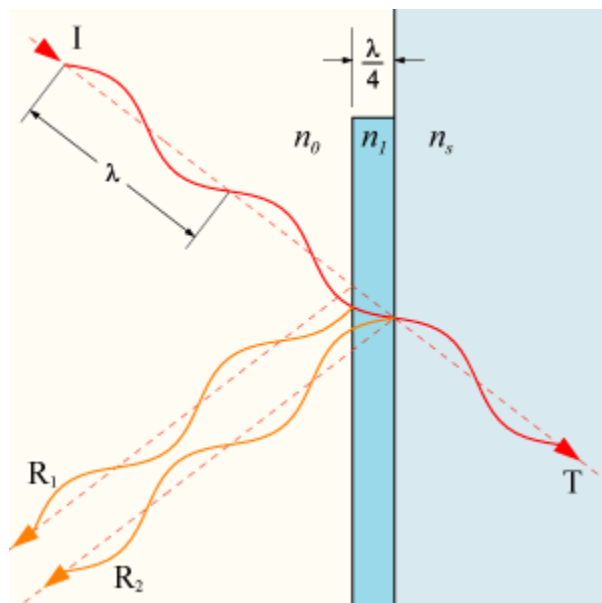
This optimum value is given by the geometric mean of the two surrounding indices:

$$n_1 = \sqrt{n_0 n_s}$$

For the example of glass ( $n_s \approx 1.5$ ) in air ( $n_0 \approx 1.0$ ), this optimum refractive index is  $n_1 \approx 1.225$ . The reflection loss of each interface is approximately 1.0% (with a combined loss of 2.0%), and an overall transmission  $T_{1s}T_{01}$  of approximately 98%. Therefore an intermediate coating between the air and glass can halve the reflection loss.

### Interference coatings

The use of an intermediate layer to form an antireflection coating can be thought of as analogous to the technique of impedance matching of electrical signals. (A similar method is used in fibre optic research where an index matching oil is sometimes used to temporarily defeat total internal reflection so that light may be coupled into or out of a fiber.) Further reduced reflection could in theory be made by extending the process to several layers of material, gradually blending the refractive index of each layer between



the index of the air and the index of the substrate.

Practical antireflection coatings, however, rely on an intermediate layer not only for its direct reduction of reflection coefficient, but also use the interference effect of a thin layer. Assume the layer thickness is controlled precisely, such that it is exactly one quarter of the light's wavelength thick ( $\lambda/4$ ). The layer is then called a quarter-wave coating. For this type of coating the incident beam I, when reflected from the second interface, will travel exactly half its

own wavelength further than the beam reflected from the first surface. If the intensities of the two beams  $R_1$  and  $R_2$  are exactly equal, they will destructively interfere and cancel each other since they are exactly out of phase. Therefore, there is no reflection from the surface, and all the energy of the beam must be in the transmitted ray,  $T$ . In the calculation of the reflection from a stack of layers, the transfer-matrix method can be used.

Real coatings do not reach perfect performance, though they are capable of reducing a surface's reflection coefficient to less than 0.1%. Practical details include correct calculation of the layer thickness; since the wavelength of the light is reduced inside a medium, this thickness will be  $\lambda_0 / 4n_1$ , where  $\lambda_0$  is the vacuum wavelength. Also, the layer will be the ideal thickness for only one distinct wavelength of light. Other difficulties include finding suitable materials for use on ordinary glass, since few useful substances have the required refractive index ( $n \approx 1.23$ ) which will make both reflected rays exactly equal in intensity. Magnesium fluoride ( $MgF_2$ ) is often used, since this is hard-wearing and can be easily applied to substrates using physical vapour deposition, even though its index is higher than desirable ( $n=1.38$ ).

Further reduction is possible by using multiple coating layers, designed such that reflections from the surfaces undergo maximum destructive interference. One way to do this is to add a second quarter-wave thick higher-index layer between the low-index layer and the substrate. The reflection from all three interfaces produces destructive interference and antireflection. Other techniques use varying thicknesses of the coatings. By using two or more layers, each of a material chosen to give the best possible match of the desired refractive index and dispersion, broadband antireflection coatings which cover the visible range (400-700 nm) with maximum reflectivities of less than 0.5% are commonly achievable.

The exact nature of the coating determines the appearance of the coated optic; common AR coatings on eyeglasses and photographic lenses often look somewhat bluish (since they reflect slightly more blue light than other visible wavelengths), though green and pink-tinged coatings are also used.

If the coated optic is used at non-normal incidence (that is, with light rays not perpendicular to the surface), the antireflection capabilities are degraded somewhat. This occurs because the phase accumulated in the layer relative to the phase of the light immediately reflected decreases as the angle increases from normal. This is counterintuitive, since the ray experiences a greater total phase shift in the layer than for normal incidence. This paradox is resolved by noting that the ray will exit the layer spatially offset from where it entered, and will interfere with reflections from incoming rays that had to travel further (thus accumulating more phase of their own) to arrive at the interface. The net effect is that the relative phase is actually reduced, shifting the coating, such that the anti-reflection band of the coating tends to move to shorter wavelengths as the optic is tilted. Non-normal incidence angles also usually cause the reflection to be polarization dependent.

### **Photonic crystals**

Photonic crystals are composed of periodic dielectric or metallo-dielectric nanostructures that affect the propagation of electromagnetic waves (EM) in the same way as the periodic potential in a semiconductor crystal affects the electron motion



by defining allowed and forbidden electronic energy bands. Essentially, photonic crystals contain regularly repeating internal regions of high and low dielectric constant. Photons (behaving as waves) propagate through this structure - or not - depending on their wavelength. Wavelengths of light that are allowed to travel are known as modes, and groups of allowed modes form bands. Disallowed bands of wavelengths are called photonic band gaps. This gives rise to distinct optical phenomena such as inhibition of spontaneous emission, high-reflecting omni-directional mirrors and low-loss-waveguiding, amongst others. Since the basic physical phenomenon is based on diffraction, the periodicity of the photonic crystal structure has to be of the same length-scale as half the wavelength of the EM waves i.e. ~200 nm (blue) to 350 nm (red) for photonic crystals operating in the visible part of the spectrum - the repeating regions of high and low dielectric constants have to be of this dimension. This makes the fabrication of optical photonic crystals cumbersome and complex.

The exploitation of electronic crystals has been one of the most important revolutions in the history of engineering and has driven the development of modern physics as we know it. The quantum theories explaining the mechanics of electrons in different materials have been a source of inspiration for scientists investigating the interaction between photons and matter. Interest in controlling material radiation has resulted in the conception of a new class of materials capable of interacting with electromagnetic waves at a structural level: they are called photonic crystals or photonic bandgap materials.

### **History of photonic crystals**

Although photonic crystals have been studied in one form or another since 1887, the term “photonic crystal” was first used over 100 years later, after Eli Yablonovitch and Sajeev John published two milestone papers on photonic crystals in 1987. Before 1987, one-dimensional photonic crystals in the form of periodic multi-layers dielectric stacks (such as the Bragg mirror) were studied extensively. Lord Rayleigh started their study in 1887, by showing that such systems have a one-dimensional photonic band-gap, a spectral range of large reflectivity, known as a stop-band. Today, such structures are used in a diverse range of applications; from reflective coatings to enhancing the efficiency of LEDs to highly reflective mirrors in certain laser cavities.

Purcell in 1946 indicated that spontaneous emission of radio waves from nuclear spin levels could be controlled by a dispersion of small metallic particles in a nuclear-magnetic material, which would create a resonant oscillator. In 1972 Bykov considered that spontaneous emission of atoms at optical wavelengths could be reduced by placing them in a periodic lattice of dielectrics with pitches smaller than the radiation wavelength, thus avoiding decay of excited states through the presence of opaque bands for the transition radiation and consequent generation of a dynamic state. Bykov also speculated as to what could happen if two- or three-dimensional periodic optical structures were used. However, these ideas did not take off until after the publication of two milestone papers in 1987 by Yablonovitch and John. Both these papers concerned high dimensional periodic optical structures – photonic crystals. Yablonovitch’s main motivation was to engineer the photonic density of states, in order to control the spontaneous emission of materials embedded within the photonic crystal; John’s idea

was to use photonic crystals to affect the localisation and control of light. Both these works addressed the engineering of a structured material exhibiting ranges of frequencies at which the propagation of electromagnetic waves is not allowed, so called bandgaps, and their employment in the emission control of optically active materials.

After 1987, the number of research papers concerning photonic crystals began to grow exponentially. However, due to the difficulty of actually fabricating these structures at optical scales, early studies were either theoretical or in the microwave regime, where photonic crystals can be built on the far more readily accessible centimetre scale. (This fact is due to a property of the electromagnetic fields known as scale invariance – in essence, the electromagnetic fields, as the solutions to Maxwell's equations, has no natural length scale, and so solutions for centimetre scale structure at microwave frequencies are the same as for nanometre scale structures at optical frequencies.) By 1991, Yablonovitch had demonstrated the first three-dimensional photonic band-gap in the microwave regime. In 1996, Thomas Krauss made the first demonstration of a two-dimensional photonic crystal at optical wavelengths. This opened up the way for photonic crystals to be fabricated in semiconductor materials by borrowing the methods used in the semiconductor industry. Today, such techniques use photonic crystal slabs, which are two dimensional photonic crystals “etched” into slabs of semiconductor; total internal reflection confines light to the slab, and allows photonic crystal effects, such as engineering the photonic dispersion to be used in the slab. Research is underway around the world to use photonic crystal slabs in integrated computer chips, in order to improve the optical processing of communications both on-chip and between chips. Although such techniques are still to mature into commercial applications, two-dimensional photonic crystals have found commercial use in the form of photonic crystal fibres (otherwise known as holey fibres, because of the air holes that run through them). Photonic crystal fibres were first developed by Philip Russell in 1998, and can be designed to possess enhanced properties over (normal) optical fibres.

[1] Purcell EM, “Spontaneous emission probabilities at radio frequencies”, Proceedings of the American Physical Society in Physical Review, 69, 681 (1946)

[2] Bykov VP, “Spontaneous emission in a periodic structure”, Soviet Physics JETP, 35, 269–273 (1972)

[3] Yablonovich E, “Inhibited spontaneous emission in solid-state physics and electronics”, Physical Review Letters, 58, 2059–2062 (1987)

[4] John S, “Strong localization of photons in certain disordered dielectric superlattices”, Physical Review Letters, 58, 2486–2489 (1987)

### **Modelling photonic crystals and computing photonic band structure**

Photonic crystals are essentially bulk materials, because the occurrence of the bandgap depends, amongst other things, on the modulation of the index of refraction over a large number of periods. The search for efficient bandgap materials has prompted scientists to solve Maxwell's equations within the periodic arrangement.

The photonic band gap (PBG) is essentially the gap between the air-line and the dielectric-line in the dispersion relation of the PBG system. To design photonic crystal

systems, it is essential to engineer the location and size of the bandgap; this is done by computational modeling using any of the following methods:

- Transfer-matrix method
- Plane wave expansion method.
- Finite Difference Time Domain method

### **Transfer matrix method (TMM)**

A multilayer is a stack of homogeneous thin-films with different indices of refraction and is usually modelled assuming that the arrangement of dielectric materials be invariant with respect to continuous translation in two orthogonal directions and not in the third.

The optical theory of thin-films was first presented in 1949 by Schuster [1]. The following year, Abelès [2] extended it to multilayers and formalized the computing technique called the transfer matrix method (TMM). The basic formalism yields the amplitude of the electromagnetic field of monochromatic waves reflected by and transmitted through the mentioned structure. The solution is achieved through propagation of the fields in the homogeneous layers, and the continuity of the tangential components of the electric and magnetic fields at the interfaces. Although the structure is onedimensional, propagation for non-normal incidence can be accounted for. The solutions for plane waves are in fact vectors of the three-dimensional Euclidean space propagating in a plane. With the exception of approximations in the chosen model, i.e. simplified dimensionality and initial conditions, or neglect of material parameters, this analytical method is exact.

The optical properties of stacks of thin layers proposed by Hooke and Newton [3, 4] were confirmed by the TMM calculations, showing that multilayers are characterised by high reflectivity and transmissivity over large portions of the spectrum. Interest in a wide variety of important applications of multilayers, including antireflective coatings (AR), high reflectivity dielectric mirrors and filters, has prompted scientists to use the TMM to compute new designs. It has been demonstrated how to extend the spectral region of high reflectance [5], or the range of angles at which the desired effect occurs [6], and recent studies have presented the extension of the TMM to stacks of anisotropic materials [7,8], showing how to obtain an omnidirectional reflector with existing materials. The simple form of the TMM equations applied to a periodically stratified medium [9] is convenient for systems with a large number of layers, but novel developments in the study of periodic structures have offered new approaches for the investigation of periodic multilayers. These techniques involve decomposition of the field into periodic modes [10], and assume infinitely extended modulations of the index. These techniques therefore cannot model effects related to the finiteness of a multilayer or the interaction of light at its boundary with the incident medium, but they have proven powerful tools to investigate an important property of dielectric stacks: the photonic bandgap [11].

Pendry et al. [12] suggested an approximative finite-element method (FEM) to solve Maxwell's equations over a discrete mesh of points in a simple cubic lattice. For a fixed frequency Pendry et al. propagated fields in one of the orthogonal directions of the lattice by means of an approximate wave vector and, assuming a periodic distribution, Pendry et al. applied periodic boundary conditions in the planes normal to the propagation direction. This resulted in a two-dimensional transfer matrix method (TMM) for the real space fields, which was successively upgraded to its Fourier-space form, to work in the resonance domain of frequencies, and was capable of fast and accurate calculation of the response of complex periodic structures [13,14].

- [1] Schuster K, "Anwendung der Vierpoltheorie auf die Probleme der optischen Reflexionsminderung, Reflexionsverstärkung und der Interferenzfilter", *Annalen der Physik*, 6, 352–356 (1949)
- [2] Abelès F, "Recherches sur la propagation des ondes electromagnetiques sinusoidales dans les milieux stratifies. Application aux couches minces", *Annales de Physique*, 5, 596–640, 706–782 (1950)
- [3] Hooke R, *Micrographia*, London: The Royal Society (1665), reprinted by Palo Alto: Octavo (1998), ISBN 1891788027.
- [4] Newton I, *Opticks*, fourth edition, London: William Innys (1730), reprinted by New York: Dover Publications (1952), ISBN 486602052
- [5] Turner AF, Baumeister PW, "Multilayer mirrors with high reflectance over an extended spectral region", *Applied Optics*, 5, 69–76 (1966)
- [6] Weber MF, Stover CA, Gilbert LR, Nevitt TJ, Ouderkirk AJ, "Giant birefringent optics in multilayer polymer mirrors", *Science*, 287, 2451–2456 (2000)
- [7] Abdulhalim I, "Omnidirectional reflection from anisotropic periodic dielectric stack", *Optics Communications*, 174, 43–50 (2000)
- [8] Cojocar J, "Forbidden gaps in periodic anisotropic layered media", *Applied Optics*, 39, 4641–4648 (2000)
- [9] Born M, Wolf E, *Principles of Optics*, seventh edition, Cambridge: Cambridge University Press (1999), ISBN 0521642221
- [10] Joannopoulos JD, Meade RD, Winn JN, *Photonic Crystals*, Princeton: Princeton University Press (1995), ISBN 0691037442
- [11] Fink Y, Winn JN, Fan S, Chen C, Michel J, Joannopoulos JD, Thomas EL, "A dielectric omnidirectional reflector", *Science*, 282, 1679–1682 (1998)
- [12] Pendry JB, MacKinnon A, "Calculation of photon dispersion relations", *Physical Review Letters*, 69, 2772–2775 (1992) 194
- [13] Pendry JB, "Photonic band structures", *Journal of Modern Optics*, 41, 209–229 (1994)
- [14] Guida G, Stavrinou PN, Parry G, Pendry JB, "Time-reversal symmetry, microcavities and photonic crystals", *Journal of Modern Optics*, 48, 581–595 (2001)

### **Plane wave method (PWM)**

Gratings have been the object of intense study ever since 18th century scientists comprehended their usefulness in optics. A grating is traditionally an evenly spaced array of straight grooves on a planar surface, and is modelled as a distribution of material (dielectric or not) periodic in one direction and invariant with respect to continuous

translation in the other. However, surface distributions periodic in two directions, found in Nature and which have also been fabricated, are often equally referred to as gratings. With gratings, the ratio between the wavelength of the interacting light and the size of their features is a crucial quantity when modelling them. Depending on the wavelength-to-pitch and wavelength-to-depth ratios of an array of diffractive elements, differing computing techniques must be adopted. Gratings with large pitches compared to the operating wavelength are called coarse, while those with a small depth-to-period ratio are termed shallow.

The scalar theory for diffraction gratings developed by Kirchhoff in the 19th century [1] has been a very successful one, but it is accurate only for coarse and shallow gratings. Modelling of gratings with large wavelength-to-pitch ratios requires a rigorous solution of Maxwell's equations. Assuming discrete translational symmetry and therefore infinite extension of the modulation, the fields decompose into periodic modes. A solution is obtained by expansion in the zone of the periodic distribution of index of refraction with periodic functions, and by energy conservation at its boundaries. The major difficulty with this method is to find a solution formulation for the scattering problem of a single diffraction element, which is also laterally periodic.

A method to rigorously obtain the diffraction of plane gratings with rectangular diffraction elements, the rigorous modal method (RMM), was proposed by Knop [2]. With the RMM, an incoming plane wave is projected onto the Fourier basis functions and substituted into the Helmholtz equation. The incident field is separated into its components parallel and perpendicular to the plane of incidence and the problems for transverse electric (TE) and transverse magnetic (TM) polarisations are solved separately. With the simultaneous Fourier expansion of the dielectric function in the periodic medium zone, this yields a standard eigenvalue problem. The direction of propagation of the modes is obtained from the solution of the eigenvalue problem, the size of which depends on the order of truncation in the expansions, and the modes are successively propagated in the periodic medium. The tangential components of the fields for all the expansion orders are then matched at the boundaries between media (usually the isotropic incidence and substrate media, and layers of periodic arrangement of dielectric) and finally the amplitudes and phases of the diffracted waves are extracted. Although this rigorous technique is in principle applicable to diffractive elements of arbitrary shape, in practice the eigenvalue problem can only be obtained for lamellar gratings because of the limitation in finding a suitable solution formulation. For both methods, numerical instabilities in the solution of the TM problem result in poor convergence and therefore poor accuracy. The instabilities are related to the Fourier expansion of the dielectric constant and are referred to as Gibbs phenomena.

Ho et al. [3] were the first to correctly predict the existence of a complete bandgap in a specific photonic crystal structure, i.e. a range of frequencies at which no propagation of waves is possible in any direction in the crystal. By means of a plane wave expansion method (PWM) they calculated the size of the bandgap for a diamond lattice of spheres, and established its dependence upon the dielectric contrast and filling fraction parameters. Ho et al. showed that a face-centered cubic lattice of spheres cannot have a complete bandgap.

The PWM is a three-dimensional version of the Fourier expansion technique mentioned when we discussed the rigorous modal method. The same difficulties have to

be addressed here as in the one-dimensional case of lamellar gratings, namely a solution for the single scatterer must be found which is periodic along the crystal axes, and numerical instabilities are encountered due to Gibb's phenomena. Analytical solutions are therefore only found for systems composed of spheres in space, and cylindrical or rectangular rods in a plane of the crystal. Convergence issues related to Gibb's phenomena are addressed using different expansion bases. Whichever the method of expansion used, the total number of terms is determined by the order of the truncation to the power of the number of dimensions in the problem.

The requirements for computation in terms of storage memory and speed of processing grow exponentially with increasing dimensionality of the problem to solve. Arbitrarily shaped "atoms" require numerical integration over the unit cell of the crystal, which is again very demanding computationally and even places many low dimensional problems beyond reach. Nevertheless, advances in this field have produced numerical methods which reduce the computational obstacles. By means of iterative optimization of an approximative initial solution, through a parallel computing approach via block matrix diagonalisation, or implementing ingenious numerical measures, such as smoothing the dielectric function[4], many previously unattainable numerical calculations have been successfully solved.

The PWM was adapted by Sakoda [5] to compute the diffraction of two-dimensional periodic bandgap materials with a finite thickness. Using a plane wave expansion in the direction of periodicity of the dielectric function and an arbitrary Fourier expansion normally to that same plane, diffracted fields were successively matched to the field expansions within the periodic medium. Predictions of the diffraction of triangular and square lattices of air rods in planar waveguides were obtained in this way with good accuracy [6,7].

- [1] Born M, Wolf E, Principles of Optics, seventh edition, Cambridge: Cambridge University Press (1999), ISBN 0521642221
- [2] Knop K, "Rigorous diffraction theory for transmission phase gratings with deep rectangular grooves", Journal of the Optical Society of America, 68, 1206–1210 (1978)
- [3] Ho KM, Chan CT, Soukoulis CM, "Existence of a Photonic Gap in Periodic Dielectric Structures", Physical Review Letters, 65, 3152–3155 (1990)
- [4] Johnson SG, Joannopoulos JD, "Block-iterative frequency-domain methods for Maxwell's equations in a planewave basis", Optics Express, 8, 173–190 (2001)
- [5] Sakoda K, "Transmittance and Bragg reflectivity of two-dimensional photonic lattices", Physical Review B, 52, 8992–9002 (1995)
- [6] Labilloy D, Benisty H, Weisbuch C, Krauss TF, De La Rue RM, Bardinal V, Houdre R, Oesterle U, Cassagne D, Jouanin C, "Quantitative measurement of transmission, reflection, and diffraction of twodimensional photonic band gap structures at near-infrared wavelengths", Physical Review Letters, 79, 4147–4150 (1997)
- [7] Benisty H, Weisbuch C, Labilloy D, Rattier M, Smith CJM, Krauss TF, De La Rue RM, Houdre R, Oesterle U, Jouanin C, Cassagne D, "Optical and confinement properties of two-dimensional photonic crystals ", Journal of Lightwave Technology, 17, 2063–2076 (1999)

### **Finite-difference time-domain (FDTD)**

Another method to solve Maxwell's equations on a discrete lattice of points in space is the finite-difference time-domain (FDTD) method. This method has a long history and has been used in a variety of applications which are reviewed in the book edited by Taflove [1]. In 1995 Chan et al. [2] were the first to apply this method to compute the band structure of photonic crystals and to prove its reliability in treating periodic structures of high complexity. The FDTD calculations are particularly useful for complicated structures because the memory and processing time requirements scale linearly with the number of grid-points included in the computation, allowing resolution of minute and intricate structures. With the FDTD method an initial field is propagated applying the governing equations in a first-order differential form, both in space and time, at all points in the grid in a succession of time steps. Different types of boundary conditions can be applied including periodic ones, particularly useful for this type of system. The fields at selected points on the grid are finally Fourier-transformed from the time to the frequency domain such that observations on spectral content can be made. Ward and Pendry [3] extended the FDTD method to nonorthogonal meshes, proved that the approximation of the equations conserves energy just as the original ones, and showed how to obtain the Green's function of a system. The FDTD method allows solution of the governing equations inside a periodic structure, but also outside at the same time, offering a tool to study the coupling of waves between different media or devices, and the diffraction or scattering of light.

[1] Taflove A, *Advances in Computational Electrodynamics: the Finitedifference Time-domain Method*, Norwood MA: Artech House (1998), ISBN 0890068348

[2] Chan CT, Yu QL, Ho KM, "Order-N spectral method for electromagnetic waves", *Physical Review B*, 51, 16635–16642 (1995)

[3] Ward AJ, Pendry JB, "Calculating photonic Green's functions using a nonorthogonal finite-difference time-domain method", *Physical Review B*, 58, 7252–7259 (1998)

### **More on Finite-difference time-domain method**

Finite-difference time-domain (FDTD) is a popular computational electrodynamics modeling technique. It is considered easy to understand and easy to implement in software. Since it is a time-domain method, solutions can cover a wide frequency range with a single simulation run.

The FDTD method belongs in the general class of grid-based differential time-domain numerical modeling methods. The time-dependent Maxwell's equations (in partial differential form) are discretized using central-difference approximations to the space and time partial derivatives. The resulting finite-difference equations are solved in either software or hardware in a leapfrog manner: the electric field vector components in a volume of space are solved at a given instant in time; then the magnetic field vector components in the same spatial volume are solved at the next instant in time; and the process is repeated over and over again until the desired transient or steady-state electromagnetic field behavior is fully evolved.

The basic FDTD space grid and time-stepping algorithm trace back to a seminal 1966 paper by Kane Yee in *IEEE Transactions on Antennas and Propagation* (Yee 1966). The descriptor "Finite-difference time-domain" and its corresponding "FDTD" acronym

were originated by Allen Taflove in a 1980 paper in IEEE Transactions on Electromagnetic Compatibility (Taflove 1980). See "References" for these and other important journal papers in the development of FDTD techniques, as well as relevant textbooks and research monographs.

Since about 1990, FDTD techniques have emerged as primary means to computationally model many scientific and engineering problems dealing with electromagnetic wave interactions with material structures. As summarized in Taflove & Hagness (2005), current FDTD modeling applications range from near-DC (ultralow-frequency geophysics involving the entire Earth-ionosphere waveguide) through microwaves (radar signature technology, antennas, wireless communications devices, digital interconnects, biomedical imaging/treatment) to visible light (photonic crystals, nanoplasmonics, solitons, and biophotonics). In 2006, an estimated 2,000 FDTD-related publications appeared in the science and engineering literature (see "Growth of FDTD publications"). At present, there are at least 27 commercial/proprietary FDTD software vendors; 8 free-software/open-source-software FDTD projects; and 2 freeware/closed-source FDTD projects, some not for commercial use.

#### *Workings of the FDTD method*

When Maxwell's differential equations are examined, it can be seen that the change in the E-field in time (the time derivative) is dependent on the change in the H-field across space (the curl). This results in the basic FDTD time-stepping relation that, at any point in space, the updated value of the E-field in time is dependent on the stored value of the E-field and the numerical curl of the local distribution of the H-field in space (Yee 1966).

The H-field is time-stepped in a similar manner. At any point in space, the updated value of the H-field in time is dependent on the stored value of the H-field and the numerical curl of the local distribution of the E-field in space. Iterating the E-field and H-field updates results in a marching-in-time process wherein sampled-data analogs of the continuous electromagnetic waves under consideration propagate in a numerical grid stored in the computer memory.

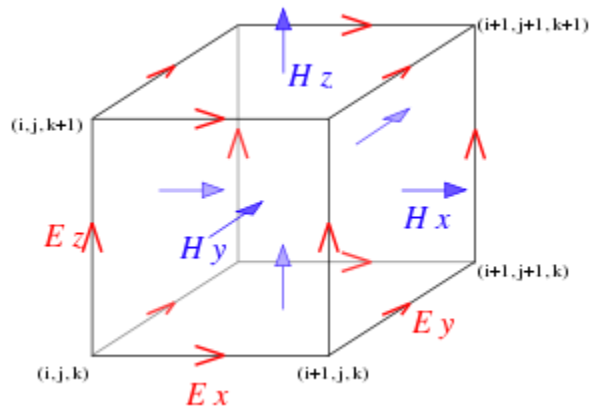


Illustration of a standard Cartesian Yee cell used for FDTD, about which electric and magnetic field vector components are distributed (Yee 1966). Visualized as a cubic voxel, the electric field components form the edges of the cube, and the magnetic field components form the normals to the faces of the cube. A three-dimensional space lattice is comprised of a multiplicity of such Yee cells. An electromagnetic wave



interaction structure is mapped into the space lattice by assigning appropriate values of permittivity to each electric field component, and permeability to each magnetic field component.

This description holds true for 1-D, 2-D, and 3-D FDTD techniques. When multiple dimensions are considered, calculating the numerical curl can become complicated. Kane Yee's seminal 1966 paper in IEEE Transactions on Antennas and Propagation proposed spatially staggering the vector components of the E-field and H-field about rectangular unit cells of a Cartesian computational grid so that each E-field vector component is located midway between a pair of H-field vector components, and conversely. This scheme, now known as a Yee lattice, has proven to be very robust, and remains at the core of many current FDTD software constructs (Yee 1966).

Furthermore, Yee proposed a leapfrog scheme for marching in time wherein the E-field and H-field updates are staggered so that E-field updates are conducted midway during each time-step between successive H-field updates, and conversely (Yee 1966). On the plus side, this explicit time-stepping scheme avoids the need to solve simultaneous equations, and furthermore yields dissipation-free numerical wave propagation. On the minus side, this scheme mandates an upper bound on the time-step to ensure numerical stability (Taflove & Brodwin 1975). As a result, certain classes of simulations can require many thousands of time-steps for completion.

#### *Using the FDTD method*

In order to use FDTD a computational domain must be established. The computational domain is simply the physical region over which the simulation will be performed. The E and H fields are determined at every point in space within that computational domain. The material of each cell within the computational domain must be specified. Typically, the material is either free-space (air), metal, or dielectric. Any material can be used as long as the permeability, permittivity, and conductivity are specified.

Once the computational domain and the grid materials are established, a source is specified. The source can be an impinging plane wave, a current on a wire, or an applied electric field, depending on the application.

Since the E and H fields are determined directly, the output of the simulation is usually the E or H field at a point or a series of points within the computational domain. The simulation evolves the E and H fields forward in time. Processing may be done on the E and H fields returned by the simulation. Data processing may also occur while the simulation is ongoing. While the FDTD technique computes electromagnetic fields within a compact spatial region, scattered and/or radiated far fields can be obtained via near-to-far-field transformations, as reported originally by Umashankar and Taflove (1982).

#### *Strengths of FDTD modeling*

Every modeling technique has strengths and weaknesses, and the FDTD method is no different. FDTD is a versatile modeling technique used to solve Maxwell's equations. It is intuitive, so users can easily understand how to use it and know what to expect from a given model.

FDTD is a time-domain technique, and when a broadband pulse (such as a Gaussian pulse) is used as the source, then the response of the system over a wide range of frequencies can be obtained with a single simulation. This is useful in applications

where resonant frequencies are not exactly known, or anytime that a broadband result is desired.

Since FDTD calculates the E and H fields everywhere in the computational domain as they evolve in time, it lends itself to providing animated displays of the electromagnetic field movement through the model. This type of display is useful in understanding what is going on in the model, and to help ensure that the model is working correctly.

The FDTD technique allows the user to specify the material at all points within the computational domain. A wide variety of linear and nonlinear dielectric and magnetic materials can be naturally and easily modeled.

FDTD allows the effects of apertures to be determined directly. Shielding effects can be found, and the fields both inside and outside a structure can be found directly or indirectly.

FDTD uses the E and H fields directly. Since most EMI/EMC modeling applications are interested in the E and H fields, it is convenient that no conversions must be made after the simulation has run to get these values.

#### *Weaknesses of FDTD modeling*

Since FDTD requires that the entire computational domain be gridded, and the grid spatial discretization must be sufficiently fine to resolve both the smallest electromagnetic wavelength and the smallest geometrical feature in the model, very large computational domains can be developed, which results in very long solution times. Models with long, thin features, (like wires) are difficult to model in FDTD because of the excessively large computational domain required.

FDTD finds the E/H fields directly everywhere in the computational domain. If the field values at some distance are desired, it is likely that this distance will force the computational domain to be excessively large. Far-field extensions are available for FDTD, but require some amount of postprocessing (Taflove & Hagness 2005).

Since FDTD simulations calculate the E and H fields at all points within the computational domain, the computational domain must be finite to permit its residence in the computer memory. In many cases this is achieved by inserting artificial boundaries into the simulation space. Care must be taken to minimize errors introduced by such boundaries. There are a number of available highly effective absorbing boundary conditions (ABCs) to simulate an infinite unbounded computational domain (Taflove & Hagness 2005). Most modern FDTD implementations instead use a special absorbing "material", called a perfectly matched layer (PML) to implement absorbing boundaries (Berenger 1994, Gedney 1996).

Because FDTD is solved by propagating the fields forward in the time domain, the electromagnetic time response of the medium must be modeled explicitly. For an arbitrary response, this involves a computationally expensive time convolution, although in most cases the time response of the medium (or Dispersion (optics)) can be adequately and simply modeled using either the recursive convolution (RC) technique, the auxiliary differential equation (ADE) technique, or the Z-transform technique. An alternative way of solving Maxwell's equations that can treat arbitrary dispersion easily is the Pseudospectral Spatial-Domain method (PSSD), which instead propagates the fields forward in space.

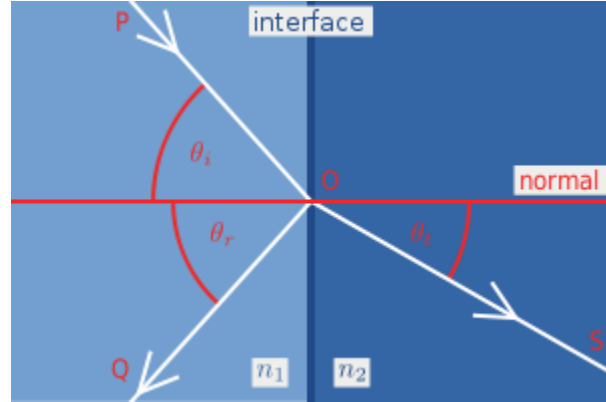
## Transfer-matrix method

### Fresnel equations

The Fresnel equations, deduced by Augustin-Jean Fresnel, describe the behaviour of light when moving between media of differing refractive indices.

When light moves from a medium of a given refractive index  $n_1$  into a second medium with refractive index  $n_2$ , both reflection and refraction of the light may occur.

In the diagram on the right, an incident light ray PO strikes at point O the interface between two media of refractive indexes  $n_1$  and  $n_2$ . Part of the ray is reflected as ray OQ and part refracted as ray OS. The angles that the incident, reflected and refracted rays make to the normal of the interface are given as  $\theta_i$ ,  $\theta_r$  and  $\theta_t$ , respectively. The relationship between these angles is given by the law of reflection and Snell's law.



The fraction of the incident power that is reflected from the interface is given by the reflection coefficient R, and the fraction that is refracted is given by the transmission coefficient T. The media are assumed to be non-magnetic.

The calculations of R and T depend on polarisation of the incident ray. If the light is polarised with the electric field of the light perpendicular to the plane of the diagram above (s-polarised), the reflection coefficient is given by:

$$R_s = \left[ \frac{\sin(\theta_t - \theta_i)}{\sin(\theta_t + \theta_i)} \right]^2 = \left[ \frac{n_1 \cos(\theta_i) - n_2 \cos(\theta_t)}{n_1 \cos(\theta_i) + n_2 \cos(\theta_t)} \right]^2 = \left[ \frac{n_1 \cos(\theta_i) - n_2 \sqrt{1 - \left(\frac{n_1}{n_2} \sin \theta_i\right)^2}}{n_1 \cos(\theta_i) + n_2 \sqrt{1 - \left(\frac{n_1}{n_2} \sin \theta_i\right)^2}} \right]^2$$

where  $\theta_t$  can be derived from  $\theta_i$  by Snell's law and is simplified using trigonometric identities.

If the incident light is polarised in the plane of the diagram (p-polarised), the R is given by:

$$R_p = \left[ \frac{\tan(\theta_t - \theta_i)}{\tan(\theta_t + \theta_i)} \right]^2 = \left[ \frac{n_1 \cos(\theta_t) - n_2 \cos(\theta_i)}{n_1 \cos(\theta_t) + n_2 \cos(\theta_i)} \right]^2 = \left[ \frac{n_1 \sqrt{1 - \left(\frac{n_1}{n_2} \sin \theta_i\right)^2} - n_2 \cos(\theta_i)}{n_1 \sqrt{1 - \left(\frac{n_1}{n_2} \sin \theta_i\right)^2} + n_2 \cos(\theta_i)} \right]^2$$

The transmission coefficient in each case is given by  $T_s = 1 - R_s$  and  $T_p = 1 - R_p$ .

If the incident light is unpolarised (containing an equal mix of s- and p-polarisations), the reflection coefficient is  $R = (R_s + R_p)/2$ .

Equations for coefficients corresponding to ratios of the electric field amplitudes of the waves can also be derived, and these are also called "Fresnel equations".

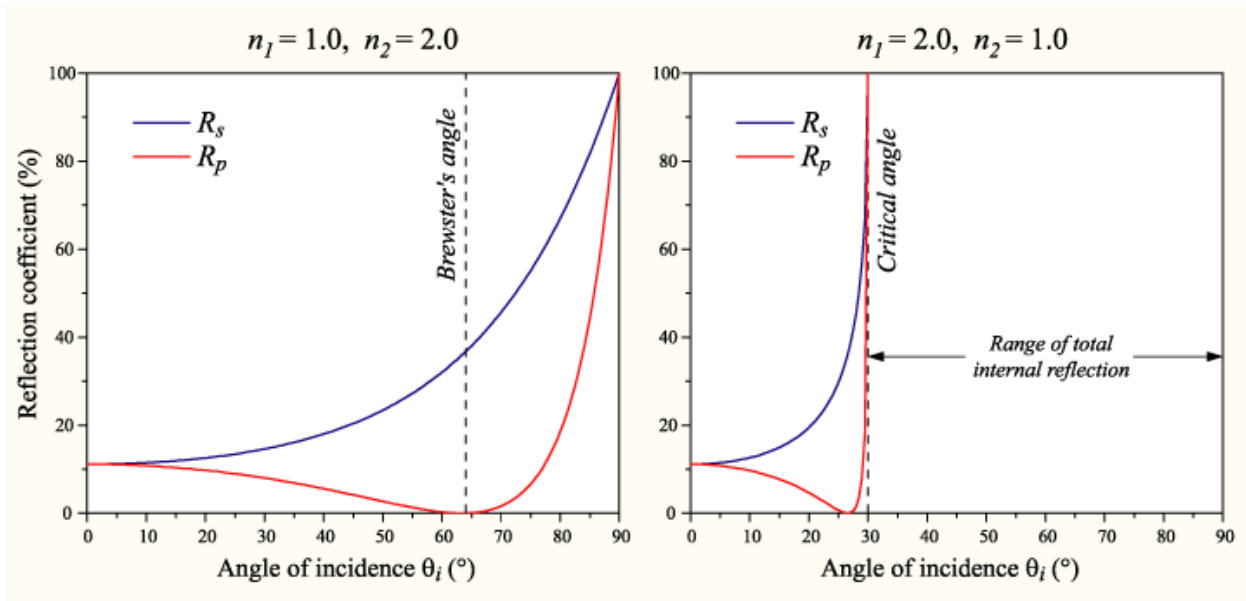
At one particular angle for a given  $n_1$  and  $n_2$ , the value of  $R_p$  goes to zero and a p-polarised incident ray is purely refracted. This angle is known as Brewster's angle, and is around  $56^\circ$  for a glass medium in air or vacuum. Note that this statement is only true when the refractive indexes of both materials are real numbers, as is the case for materials like air and glass.

For materials that absorb light, like metals and semiconductors,  $n$  is complex, and  $R_p$  does not generally go to zero.

When moving from a denser medium into a less dense one (i.e.,  $n_1 > n_2$ ), above an incidence angle known as the critical angle, all light is reflected and  $R_s = R_p = 1$ . This phenomenon is known as total internal reflection. The critical angle is approximately  $41^\circ$  for glass in air.

When the light is at near-normal incidence to the interface ( $\theta_i \approx \theta_t \approx 0$ ), the reflection and transmission coefficient are given by:

$$R = R_s = R_p = \left( \frac{n_1 - n_2}{n_1 + n_2} \right)^2 \quad T = T_s = T_p = 1 - R = \frac{4n_1 n_2}{(n_1 + n_2)^2}$$



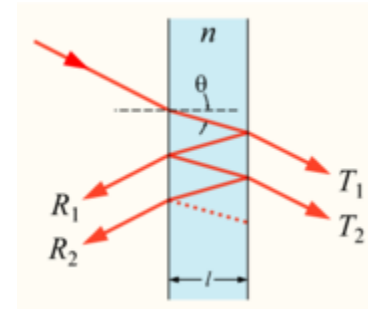
For common glass, the reflection coefficient is about 4%. Note that reflection by a window is from the front side as well as the back side, and that some of the light bounces back and forth a number of times between the two sides. The combined reflection coefficient for this case is  $2R/(1 + R)$ , when interference can be neglected. (See below.)

It should be noted that the discussion given here assumes that the permeability  $\mu$  is equal to the vacuum permeability  $\mu_0$  in both media. This is approximately true for most dielectric materials, but not for some other types of material. The completely general Fresnel equations are more complicated.

### Transfer-matrix method

The transfer-matrix method is a method used in optics and acoustics to analyze the propagation of electromagnetic or acoustic waves through a stratified (layered) medium. This is for example relevant for the design of anti-reflective coatings and dielectric mirrors.

The reflection of light from a single interface between two media is described by the Fresnel equations. However, when there are multiple interfaces, such as in the figure, the reflections themselves are also partially reflected. Depending on the exact path length, these reflections can interfere destructively or constructively. The overall reflection of a layer structure is the sum of an infinite number of reflections, which is cumbersome to calculate.



The transfer-matrix method is based on the fact that, according to Maxwell's equations, there are simple continuity conditions for the electric field across boundaries from one medium to the next. If the field is known at the beginning of a layer, the field at the end of the layer can be derived from a simple matrix operation. A stack of layers can then be represented as a system matrix, which is the product of the individual layer matrices. The final step of the method involves converting the system matrix back into reflection and transmission coefficients.

Below is described how the transfer matrix is applied to electromagnetic waves (for example light) of a given frequency propagating through a stack of layers at normal incidence. It can be generalized to deal with incidence at an angle, absorbing media, and media with magnetic properties. We assume that the stack layers are normal to the  $z$  axis and that the field within one layer can be represented as the superposition of a left- and right-traveling wave with wave number  $k$ ,

$$E(z) = E_r e^{ikz} + E_l e^{-ikz}$$

Because it follows from Maxwell's equation that  $E$  and  $F = dE/dz$  must be continuous across a boundary, it is convenient to represent the field as the vector  $(E(z), F(z))$ , where

$$F(z) = ikE_r e^{ikz} - ikE_l e^{-ikz}$$

Since there are two equations relating  $E$  and  $F$  to  $E_r$  and  $E_l$ , these two representations are equivalent. In the new representation, propagation over a distance  $L$  into the positive  $z$  direction is described by the matrix

$$M = \begin{pmatrix} \cos kL & \frac{1}{k} \sin kL \\ -k \sin kL & \cos kL \end{pmatrix},$$

and

$$\begin{pmatrix} E(z+L) \\ F(z+L) \end{pmatrix} = M \cdot \begin{pmatrix} E(z) \\ F(z) \end{pmatrix}$$

Such a matrix can represent propagation through a layer if  $k$  is the wave number in the medium and  $L$  the thickness of the layer: For a system with  $N$  layers, each layer  $J$  has a transfer matrix  $M_J$ , where  $J$  increases towards higher  $z$  values. The system transfer matrix is then

$$M_s = M_N \cdot \dots \cdot M_2 \cdot M_1.$$

Typically, one would like to know the reflectance and transmittance of the layer structure. If the layer stack starts at  $z = 0$ , then for negative  $z$ , the field is described as

$$E_L(z) = E_0 e^{ik_L z} + r E_0 e^{-ik_L z},$$

where  $E_0$  is the amplitude of the incoming wave,  $k_L$  the wave number in the left medium, and  $r$  is the amplitude (not intensity!) reflectance coefficient of the layer structure. On the other side of the layer structure, the field consists of a right-propagating transmitted field

$$E_R(z) = t E_0 e^{ik_R z},$$

where  $t$  is the amplitude transmittance and  $k_R$  is the wave number in the rightmost medium. If  $F_L = dE_L/dz$  and  $F_R = dE_R/dz$ , then we can solve

$$\begin{pmatrix} E(z_R) \\ F(z_R) \end{pmatrix} = M \cdot \begin{pmatrix} E(0) \\ F(0) \end{pmatrix}$$

in terms of the matrix elements  $M_{mn}$  of the system matrix  $M_s$  and obtain

$$r = \frac{-ik_R M_{11} + k_L k_R M_{12} + M_{21} + ik_L M_{22}}{-M_{21} + ik_L M_{22} + ik_R M_{11} + k_L k_R M_{12}},$$

and

$$t = \frac{(-M_{21} + ik_L M_{22})(M_{11} + ik_L M_{12}) + (M_{11} - ik_L M_{12})(M_{21} + ik_L M_{22})}{-M_{21} + ik_L M_{22} + ik_R M_{11} + k_L k_R M_{12}}$$

The intensity transmittance and reflectance, which are often of more practical use, are  $T = |t|^2$  and  $R = |r|^2$ , respectively.

### Fabry-Pérot interferometer

As an illustration, consider a single layer of glass with a refractive index  $n$  and thickness  $d$  suspended in air at a wave number  $k$  (in air). In glass, the wave number is  $k' = nk$ . The transfer matrix is

$$M = \begin{pmatrix} \cos k'd & \sin(k'd)/k' \\ -k' \sin k'd & \cos k'd \end{pmatrix}.$$

The amplitude reflection coefficient can be simplified to

$$r = \frac{(1/n - n) \sin k'd}{(n + 1/n) \sin k'd + 2i \cos(k'd)}.$$

This configuration effectively describes a Fabry-Pérot interferometer or etalon: for  $k'd = 0, \pi, 2\pi, \dots$ , the reflection vanishes.

The varying transmission function of an etalon is caused by interference between the multiple reflections of light between the two reflecting surfaces. Constructive interference occurs if the transmitted beams are in phase, and this corresponds to a high-transmission peak of the etalon. If the transmitted beams are out-of-phase, destructive interference occurs and this corresponds to a transmission minimum. Whether the multiply-reflected beams are in-phase or not depends on the wavelength ( $\lambda$ ) of the light (in vacuum), the angle the light travels through the etalon ( $\theta$ ), the thickness of the etalon ( $l$ ) and the refractive index of the material between the reflecting surfaces ( $n$ ).

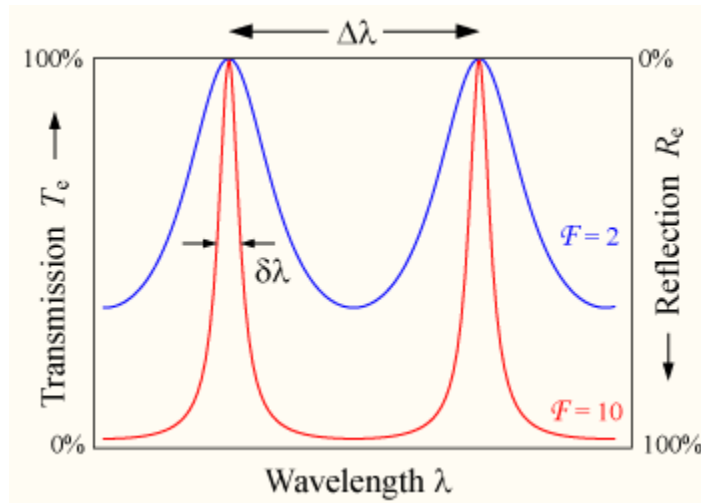
The phase difference between each succeeding reflection is given by  $\delta$ :

$$\delta = \left(\frac{2\pi}{\lambda}\right) 2nl \cos \theta.$$

If both surfaces have a reflectance  $R$ , the transmittance function of the etalon is given by:

$$T_e = \frac{(1 - R)^2}{1 + R^2 - 2R \cos(\delta)} = \frac{1}{1 + F \sin^2\left(\frac{\delta}{2}\right)}$$

where  $F = \frac{4R}{(1 - R)^2}$  is the coefficient of finesse.



The transmission of an etalon as a function of wavelength. A high-finesse etalon (red line) shows sharper peaks and lower transmission minima than a low-finesse etalon (blue).

Maximum transmission ( $T_e = 1$ ) occurs when the optical path length difference ( $2nl \cos \theta$ ) between each transmitted beam is an integer multiple of the wavelength. In the absence of

absorption, the reflectance of the etalon is the complement of the transmittance, such that  $T_e + R_e = 1$ . The maximum reflectivity is given by:

$$R_{max} = 1 - \frac{1}{1 + F} = \frac{4R}{(1 + R)^2}$$

and this occurs when the path-length difference is equal to half an odd multiple of the wavelength.

The wavelength separation between adjacent transmission peaks is called the free spectral range (FSR) of the etalon,  $\Delta\lambda$ , and is given by:

$$\Delta\lambda = \frac{\lambda_0^2}{2nl \cos \theta + \lambda_0} \approx \frac{\lambda_0^2}{2nl \cos \theta}$$

where  $\lambda_0$  is the central wavelength of the nearest transmission peak. The FSR is related to the full-width half-maximum,  $\delta\lambda$ , of any one transmission band by a quantity known as the finesse:

$$\mathcal{F} = \frac{\Delta\lambda}{\delta\lambda} = \frac{\pi}{2 \arcsin(1/\sqrt{F})}$$

This is commonly approximated (for  $R > 0.5$ ) by

$$\mathcal{F} \approx \frac{\pi\sqrt{F}}{2} = \frac{\pi R^{1/2}}{(1-R)}$$

Etalons with high finesse show sharper transmission peaks with lower minimum transmission coefficients.

A Fabry-Pérot interferometer differs from a Fabry-Pérot etalon in the fact that the distance  $l$  between the plates can be tuned in order to change the wavelengths at which transmission peaks occur in the interferometer. Due to the angle dependence of the transmission, the peaks can also be shifted by rotating the etalon with respect to the beam.

Fabry-Pérot interferometers or etalons are used in optical modems, spectroscopy, lasers, and astronomy.

#### Detailed analysis

Two beams are shown in the diagram at the right, one of which ( $T_0$ ) is transmitted through the etalon, and the other of which ( $T_1$ ) is reflected twice before being transmitted. At each reflection, the amplitude is reduced by  $\sqrt{R}$  and the phase is shifted by  $\pi$ , while at each transmission through an interface the amplitude is reduced by  $\sqrt{T}$ . Assuming no absorption, we have by conservation of energy  $T + R = 1$ . Define  $n$  as the index of refraction inside the etalon, and  $n_0$  as the index of refraction outside the etalon. Using phasors to represent the amplitude of the radiation, let's suppose that the amplitude at point a is unity. The amplitude at point b will then be

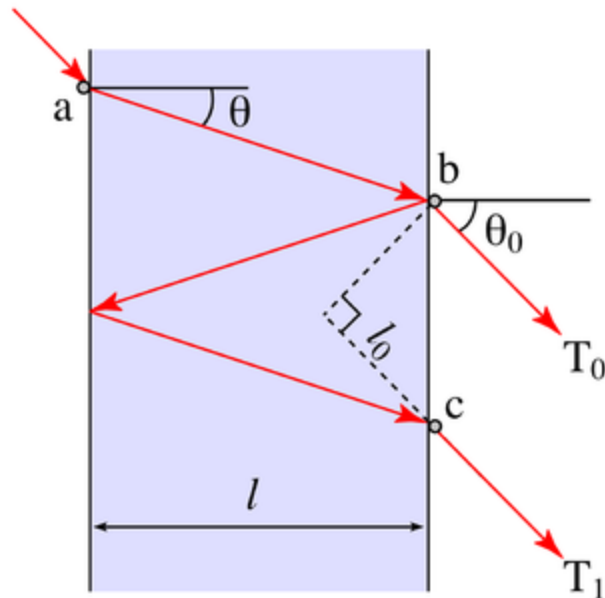
$$T_0 = T e^{ikl/\cos\theta}$$

where  $k = 2\pi/\lambda$  is the wave number inside the etalon and  $\lambda$  is the vacuum wavelength.

At point c the amplitude will be

$$TR e^{2\pi i + 3ikl/\cos\theta}$$

The total amplitude of both beams will be the sum of the amplitudes of the two beams measured along a line perpendicular to the direction of the beam. We therefore





add the amplitude at point b to an amplitude T1 equal in magnitude to the amplitude at point c, but which has been retarded in phase by an amount  $k_0 l_0$  where  $k_0 = 2\pi n_0 / \lambda$  is the wave number outside of the etalon. Thus:

$$T_1 = RT e^{2\pi i + 3ikl / \cos \theta - ik_0 l_0}$$

where  $l_0$  is seen to be:

$$l_0 = 2l \tan(\theta) \sin(\theta_0)$$

Neglecting the  $2\pi$  phase change due to the two reflections, we have for the phase difference between the two beams

$$\delta = \frac{2kl}{\cos(\theta)} - k_0 l_0$$

The relationship between  $\theta$  and  $\theta_0$  is given by Snell's law:

$$n \sin(\theta) = n_0 \sin(\theta_0)$$

So that the phase difference may be written

$$\delta = 2kl \cos(\theta)$$

To within a constant multiplicative phase factor, the amplitude of the m-th transmitted beam can be written as

$$T_m = TR^m e^{im\delta}$$

The total transmitted beam is the sum of all individual beams

$$A_T = \sum_{m=0}^{\infty} T_m = T \sum_{m=0}^{\infty} R^m e^{im\delta}$$

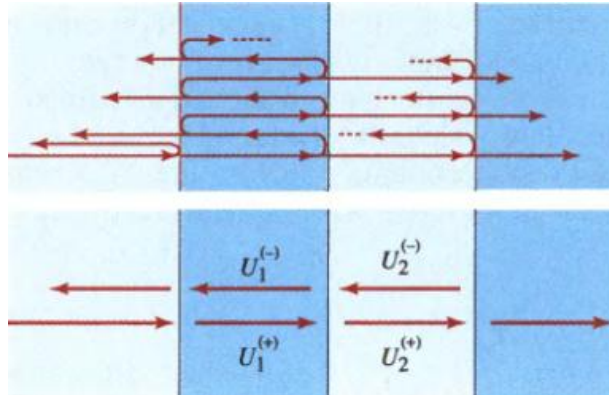
The series is a geometric series whose sum can be expressed analytically. The amplitude can be rewritten as

$$A_T = \frac{T}{1 - Re^{i\delta}}$$

The intensity of the beam will be just  $A_T A_T^*$  and, since the incident beam was assumed to have an intensity of unity, this will also give the transmission function:

$$T_e = A_T A_T^* = \frac{T^2}{1 + R^2 - 2R \cos(\delta)}$$

Transfer matrix



$$\begin{array}{c}
 U_1^{(+)} \rightarrow \\
 \leftarrow U_1^{(-)} \\
 \hline
 \boxed{\mathbf{M}} \\
 \hline
 U_2^{(+)} \rightarrow \\
 \leftarrow U_2^{(-)}
 \end{array}
 \quad
 \begin{bmatrix} U_2^{(+)} \\ U_2^{(-)} \end{bmatrix}
 =
 \begin{bmatrix} A & B \\ C & D \end{bmatrix}
 \begin{bmatrix} U_1^{(+)} \\ U_1^{(-)} \end{bmatrix}$$

Scattering matrix

$$\begin{array}{c}
 U_1^{(+)} \rightarrow \\
 \leftarrow U_2^{(-)} \\
 \leftarrow U_1^{(-)} \\
 \hline
 \boxed{\mathbf{S}} \\
 \hline
 U_2^{(+)} \rightarrow \\
 \leftarrow U_1^{(-)}
 \end{array}
 \quad
 \begin{bmatrix} U_2^{(+)} \\ U_1^{(-)} \end{bmatrix}
 =
 \begin{bmatrix} t_{12} & r_{21} \\ r_{12} & t_{21} \end{bmatrix}
 \begin{bmatrix} U_1^{(+)} \\ U_2^{(-)} \end{bmatrix}$$

$$\mathbf{M} = \begin{bmatrix} A & B \\ C & D \end{bmatrix} = \frac{1}{t_{21}} \begin{bmatrix} t_{12}t_{21} - r_{12}r_{21} & r_{21} \\ -r_{12} & 1 \end{bmatrix}$$

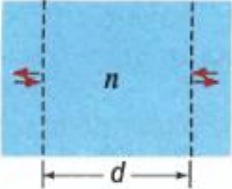
$$\mathbf{S} = \begin{bmatrix} t_{12} & r_{21} \\ r_{12} & t_{21} \end{bmatrix} = \frac{1}{D} \begin{bmatrix} AD - BC & B \\ -C & 1 \end{bmatrix}.$$

Airy's formulas

For two systems, the multiplication of two transfer-matrices  $M_{13}=M_{12}M_{23}$  gives:

$$t_{13} = \frac{t_{12}t_{23}}{1 - r_{21}r_{23}}, \quad r_{13} = r_{12} + \frac{t_{12}t_{21}r_{23}}{1 - r_{21}r_{23}}.$$

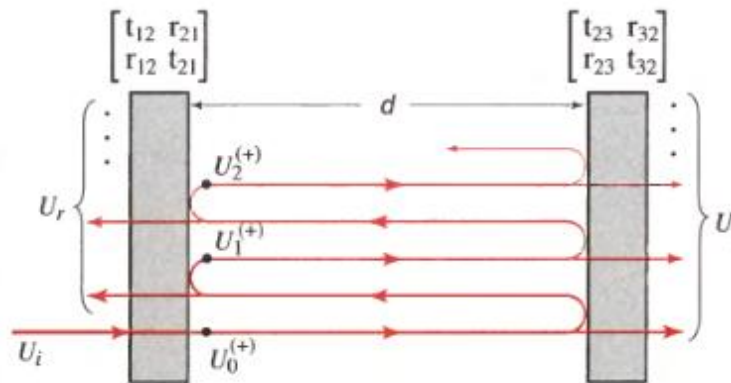
For a homogenous medium of index  $n$  and thickness  $d$  we have the transfer matrix  $M$ :



$$\mathbf{M} = \begin{bmatrix} \exp(-j\varphi) & 0 \\ 0 & \exp(j\varphi) \end{bmatrix}, \quad \mathbf{S} = \begin{bmatrix} \exp(-j\varphi) & 0 \\ 0 & \exp(-j\varphi) \end{bmatrix}, \quad \varphi = nk_0 d.$$

For two systems separated by a homogenous medium, the multiplication of transfer-matrices  $M_{13} = M_{12} M M_{23}$  gives:

$$t_{13} = \frac{t_{12} t_{23} \exp(-j\varphi)}{1 - r_{21} r_{23} \exp(-j2\varphi)}, \quad r_{13} = r_{12} + \frac{t_{12} t_{21} r_{23} \exp(-j2\varphi)}{1 - r_{21} r_{23} \exp(-j2\varphi)}$$



## References

Photonic crystals

[http://en.wikipedia.org/wiki/Photonic\\_crystal](http://en.wikipedia.org/wiki/Photonic_crystal)

[http://www.ee.ucla.edu/labs/photon/eliy\\_SCIAM.pdf](http://www.ee.ucla.edu/labs/photon/eliy_SCIAM.pdf)

<http://www.ee.ucla.edu/labs/photon/pubs/ey2007opn183.pdf>

J. D. Joannopoulos, S. G. Johnson, J.N. Winn, R. D. Meade, Photonic Crystals: Molding the Flow of Light, 2nd ed. , Princeton University Press, Princeton, NJ, 2008.

<http://ab-initio.mit.edu/book/photonic-crystals-book.pdf>

<http://ab-initio.mit.edu/photons/tutorial/>

Fresnel equations

[http://en.wikipedia.org/wiki/Fresnel\\_equations](http://en.wikipedia.org/wiki/Fresnel_equations)

[http://phys.ubbcluj.ro/~evinteler/nanofotonica/Fresnel\\_Sernelius.pdf](http://phys.ubbcluj.ro/~evinteler/nanofotonica/Fresnel_Sernelius.pdf)

<http://www.ifm.liu.se/~boser/elma/Lect12.pdf>

TTM method

Saleh B.E.A., Teich M.C. Fundamentals of Photonics, Wiley, 2ed, 2007, chap.7  
[http://en.wikipedia.org/wiki/Transfer-matrix\\_method\\_\(optics\)](http://en.wikipedia.org/wiki/Transfer-matrix_method_(optics))  
[http://phys.ubbcluj.ro/~evinteler/nanofotonica/TTM\\_Sernelius.pdf](http://phys.ubbcluj.ro/~evinteler/nanofotonica/TTM_Sernelius.pdf)  
<http://www.ifm.liu.se/~boser/elma/Lect13.pdf>

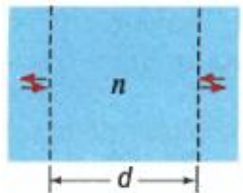
Program Translight and manual written by A.Reynolds  
[http://phys.ubbcluj.ro/~evinteler/nanofotonica/translight\\_manual\\_Reynolds.pdf](http://phys.ubbcluj.ro/~evinteler/nanofotonica/translight_manual_Reynolds.pdf)  
<http://phys.ubbcluj.ro/~evinteler/nanofotonica/programs>

Based on Saleh B.E.A., Teich M.C. Fundamentals of Photonics, Wiley, 2ed, 2007, chap.7

### Evaluation tests

#### 1. Homogeneous medium

For a homogeneous medium of index  $n$  and thickness  $d$  show that the transfer matrix  $M$  is:



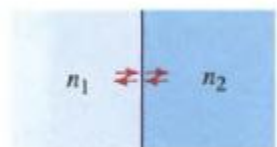
$$\mathbf{M} = \begin{bmatrix} \exp(-j\varphi) & 0 \\ 0 & \exp(j\varphi) \end{bmatrix}, \mathbf{S} = \begin{bmatrix} \exp(-j\varphi) & 0 \\ 0 & \exp(-j\varphi) \end{bmatrix}, \varphi = nk_0 d.$$

Hint: Use the definition of scattering matrix  $S$  and determine the reflection and transmission coefficients with Fresnel equations.

#### 2. Single Dielectric Boundary

Show that at the boundary between two media of refractive indexes  $n_1$  and  $n_2$  the scattering and transfer matrix is:

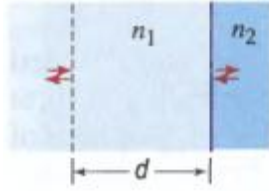
$$\mathbf{S} = \begin{bmatrix} t_{12} & r_{21} \\ r_{12} & t_{21} \end{bmatrix} = \frac{1}{n_1 + n_2} \begin{bmatrix} 2n_1 & n_2 - n_1 \\ n_1 - n_2 & 2n_2 \end{bmatrix}$$



$$\mathbf{M} = \frac{1}{2n_2} \begin{bmatrix} n_2 + n_1 & n_2 - n_1 \\ n_2 - n_1 & n_2 + n_1 \end{bmatrix}$$

#### 3. Propagation Followed by a Boundary

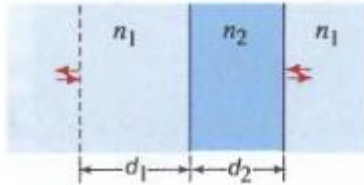
Show that for a homogeneous medium followed by the boundary between two media of refractive indexes  $n_1$  and  $n_2$  the scattering and transfer matrix is:



$$\mathbf{M} = \frac{1}{2n_2} \begin{bmatrix} (n_2 + n_1) e^{-j\varphi} & (n_2 - n_1) e^{j\varphi} \\ (n_2 - n_1) e^{-j\varphi} & (n_2 + n_1) e^{j\varphi} \end{bmatrix}, \quad \varphi = n_1 k_o d.$$

#### 4. Propagation Followed by Transmission Through a Slab.

Show that for a two homogeneous media with refractive indexes  $n_1$  and  $n_2$  and thicknesses  $d_1$  and  $d_2$  the transfer matrix is:



$$\mathbf{M} = \frac{1}{4n_1 n_2} \begin{bmatrix} (n_1 + n_2) e^{-j\varphi_2} & (n_1 - n_2) e^{j\varphi_2} \\ (n_1 - n_2) e^{-j\varphi_2} & (n_1 + n_2) e^{j\varphi_2} \end{bmatrix} \times \begin{bmatrix} (n_2 + n_1) e^{-j\varphi_1} & (n_2 - n_1) e^{j\varphi_1} \\ (n_2 - n_1) e^{-j\varphi_1} & (n_2 + n_1) e^{j\varphi_1} \end{bmatrix}$$

where:

$$\varphi_1 = n_1 k_o d_1 \text{ and } \varphi_2 = n_2 k_o d_2.$$

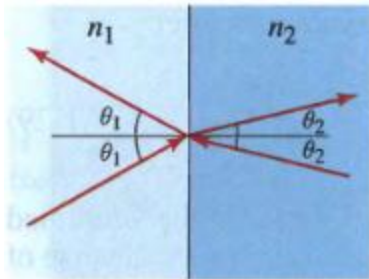
and transmission coefficient is:

$$t = \exp(-j\varphi_1) \frac{4n_1 n_2 \exp(-j\varphi_2)}{(n_1 + n_2)^2 - (n_1 - n_2)^2 \exp(-j2\varphi_2)}$$

Hint: Use the relation between the scattering and transfer matrices.

#### 5. Single Dielectric Boundary. Oblique TE and TM waves

Show that a wave transmitted through a planar boundary between media of refractive indexes  $n_1$  and  $n_2$  at angles  $\theta_1$  and  $\theta_2$ , satisfying Snell's law ( $n_1 \sin \theta_1 = n_2 \sin \theta_2$ ), is described by a scattering and transfer matrix determined from the Fresnel equations:



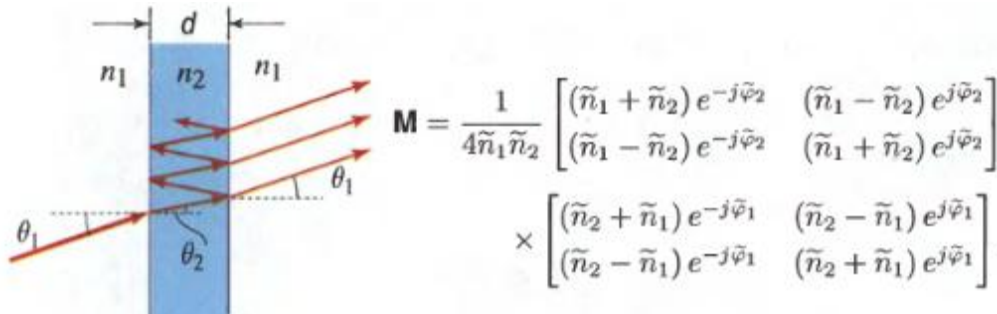
$$\mathbf{S} = \begin{bmatrix} t_{12} & r_{21} \\ r_{12} & t_{21} \end{bmatrix} = \frac{1}{\tilde{n}_1 + \tilde{n}_2} \begin{bmatrix} 2a_{12}\tilde{n}_1 & \tilde{n}_2 - \tilde{n}_1 \\ \tilde{n}_1 - \tilde{n}_2 & 2a_{21}\tilde{n}_2 \end{bmatrix}$$

$$\mathbf{M} = \begin{bmatrix} A & B \\ C & D \end{bmatrix} = \frac{1}{2a_{21}\tilde{n}_2} \begin{bmatrix} \tilde{n}_1 + \tilde{n}_2 & \tilde{n}_2 - \tilde{n}_1 \\ \tilde{n}_2 - \tilde{n}_1 & \tilde{n}_1 + \tilde{n}_2 \end{bmatrix}.$$

$$\begin{aligned} \text{TE: } & \tilde{n}_1 = n_1 \cos \theta_1, \quad \tilde{n}_2 = n_2 \cos \theta_2, \quad a_{12} = a_{21} = 1, \\ \text{TM: } & \tilde{n}_1 = n_1 \sec \theta_1, \quad \tilde{n}_2 = n_2 \sec \theta_2, \quad a_{12} = \cos \theta_1 / \cos \theta_2 = 1/a_{21}. \end{aligned}$$

#### 6. Off-axis Propagation Followed by Transmission Through a Slab.

Show that for a slab with thickness  $d$  and refractive indexes  $n_2$  between two homogeneous media with refractive index  $n_1$ , the transfer matrix is:



where for TE waves, respectively TM waves we have:

$$\begin{aligned} \text{TE:} \quad & \tilde{n}_1 = n_1 \cos \theta_1, \quad \tilde{n}_2 = n_2 \cos \theta_2, \quad \tilde{\varphi}_1 = n_1 k_o d_1 \cos \theta_1 \\ \text{TM:} \quad & \tilde{n}_1 = n_1 \sec \theta_1, \quad \tilde{n}_2 = n_2 \sec \theta_2, \quad \tilde{\varphi}_2 = n_2 k_o d_2 \cos \theta_2 \end{aligned}$$

### 7. Mirror Fabry-Perot etalon

Consider two lossless partially reflective mirrors with amplitude transmittances  $t_1$  and  $t_2$  and amplitude reflectances  $r_1$  and  $r_2$  separated by a distance  $d$  filled with a medium of refractive index  $n$ . Show that for the overall system the transfer matrix is:

$$\mathbf{M} = \begin{bmatrix} 1/t_1^* & r_1/t_1 \\ r_1^*/t_1^* & 1/t_1 \end{bmatrix} \begin{bmatrix} \exp(-j\varphi) & 0 \\ 0 & \exp(j\varphi) \end{bmatrix} \begin{bmatrix} 1/t_2^* & r_2/t_2 \\ r_2^*/t_2^* & 1/t_2 \end{bmatrix}$$

Using this result show that the intensity transmittance is:

$$\mathcal{T} = |t|^2 = \frac{|t_1 t_2|^2}{|1 - r_1 r_2 \exp(-j2\varphi)|^2}$$

where:

$$\varphi = nk_o d.$$

For two identical mirrors with reflectance  $R = |r_1|^2 = |r_2|^2$  show that we have:

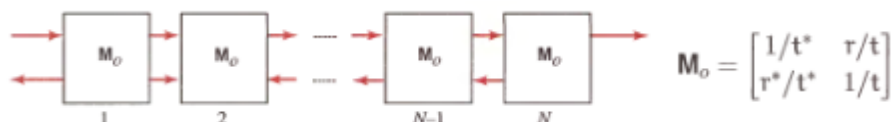
$$T_e = \frac{(1 - R)^2}{1 + R^2 - 2R \cos(\delta)} = \frac{1}{1 + F \sin^2\left(\frac{\delta}{2}\right)}$$

where:

$$\delta = \left(\frac{2\pi}{\lambda}\right) 2nl \cos \theta.$$

### 8. Bragg grating

For a system composed from  $N$  identical modules with transfer matrix  $M_o$



show that the overall transfer matrix  $M_N = M_o^N$  is:

$$\mathbf{M}_o^N = \Psi_N \mathbf{M}_o - \Psi_{N-1} \mathbf{I},$$

$$\Psi_N = \frac{\sin N\Phi}{\sin \Phi} \quad \cos \Phi = \operatorname{Re}\{1/t\}$$

Hint: Use the unimodularity of matrix  $\mathbf{M}_o$  ( $\det \mathbf{M}_o=1$ ).

Using the fact that:

$$\mathbf{M}_o^N = \begin{bmatrix} 1/t_N^* & r_N/t_N \\ r_N^*/t_N^* & 1/t_N \end{bmatrix}$$

$$\frac{1}{t_N} = \Psi_N \frac{1}{t} - \Psi_{N-1}$$

$$\frac{r_N}{t_N} = \Psi_N \frac{r}{t}$$

$$\mathcal{T}_N = \frac{\mathcal{T}}{\mathcal{T} + \Psi_N^2(1 - \mathcal{T})}, \quad \mathcal{R}_N = 1 - \mathcal{T}_N = \frac{\Psi_N^2 \mathcal{R}}{1 - \mathcal{R} + \Psi_N^2 \mathcal{R}}$$

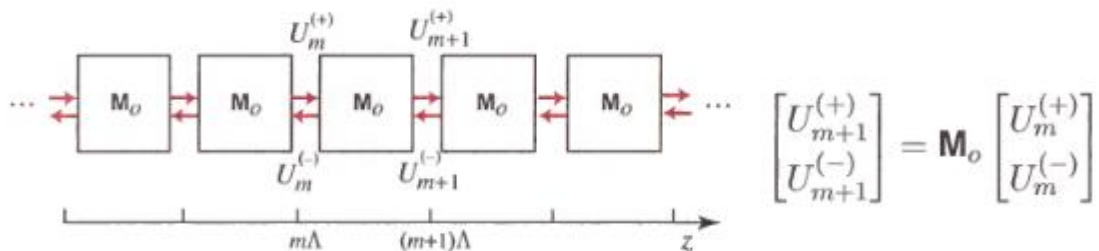
show that intensity transmittance and reflectance is:

In the limit for the reflectance of a single module show that:

$$\mathcal{R}_N \approx \Psi_N^2 \mathcal{R} = \frac{\sin^2 N\Phi}{\sin^2 \Phi} \mathcal{R}, \quad \mathcal{R} \ll 1, \quad \Psi_N^2 \mathcal{R} \ll 1$$

## 9. Periodic medium

For a periodic medium composed of identical modules described by transfer matrix  $\mathbf{M}_o$



we have the eigenmodes that satisfy relation:

$$\begin{bmatrix} U_{m+1}^{(+)} \\ U_{m+1}^{(-)} \end{bmatrix} = e^{-j\Phi} \begin{bmatrix} U_m^{(+)} \\ U_m^{(-)} \end{bmatrix}, \quad m = 1, 2, \dots; \quad \Phi = K\Lambda.$$

For  $m=0$  we have the eigenvalue problem:

$$\mathbf{M}_o \begin{bmatrix} U_0^{(+)} \\ U_0^{(-)} \end{bmatrix} = e^{-j\Phi} \begin{bmatrix} U_0^{(+)} \\ U_0^{(-)} \end{bmatrix}.$$

Show that we have (use the form of  $\mathbf{M}_o$  from previous problem):

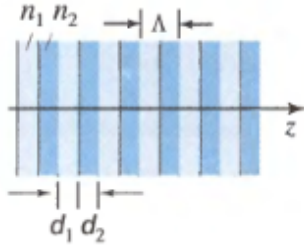
$$\cos \Phi = \operatorname{Re} \left\{ \frac{1}{t} \right\}$$

Hint: Use relations:

$$|t|^2 + |r|^2 = 1$$

$$e^{-j\Phi} = \frac{1}{2}(1/t + 1/t^*) \pm j \left\{ 1 - \left[ \frac{1}{2}(1/t + 1/t^*) \right]^2 \right\}^{1/2}$$

### 10. 1D photonic crystal: Alternating dielectric layers



Show that for the system in the figure we have the following dispersion relation:

$$\cos \left( 2\pi \frac{K}{g} \right) = \frac{1}{t_{12}t_{21}} \left[ \cos \left( \pi \frac{\omega}{\omega_B} \right) - |r_{12}|^2 \cos \left( \pi \zeta \frac{\omega}{\omega_B} \right) \right]$$

where:

$$g = 2\pi/\Lambda, \text{ and } \omega_B = c\pi/\Lambda$$

$$\omega_B = (c_0/\bar{n})(\pi/\Lambda)$$

$$\Lambda = d_1 + d_2$$

$$\bar{n} = (n_1 d_1 + n_2 d_2)/\Lambda$$

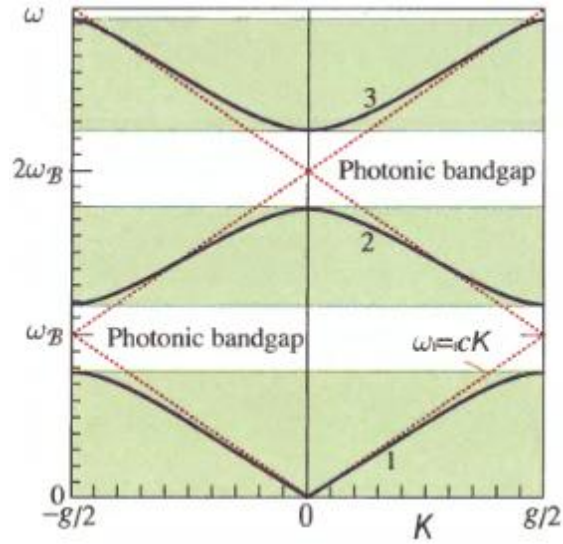
$$\zeta = (n_1 d_1 - n_2 d_2)/(n_1 d_1 + n_2 d_2)$$

$$t_{12}t_{21} = 4n_1 n_2 / (n_1 + n_2)^2$$

$$|r_{12}|^2 = (n_2 - n_1)^2 / (n_1 + n_2)^2.$$

Plot dispersion relation in coordinates  $K, \omega$  and show that we have photonic bandgaps around frequency values  $m \cdot \omega_B$  :





Hint: Use the relation obtained in the previous problem:

$$\cos \Phi = \operatorname{Re} \left\{ \frac{1}{t} \right\}$$

and replace transmission  $t$  obtained from problem 4 (Propagation Followed by Transmission Through a Slab) by phases:

$$\begin{aligned} \varphi_1 + \varphi_2 &= k_o(n_1 d_1 + n_2 d_2) = \pi \omega / \omega_B \\ \varphi_1 - \varphi_2 &= \zeta \pi \omega / \omega_B \end{aligned}$$